Earthquake Engineering, Tenth World Conference © 1992 Balkema, Rotterdam. ISBN 90 5410 060 5

Comparison of different material models in simulating masonry behaviour under horizontal loads

D. Liberatore, F. Braga & E. Mancinelli
Università degli Studi della Basilicata, Potenza, Italy

S. Mazzolani
Università Federico II, Naples, Italy

ABSTRACT: Correct modeling of panels under vertical and horizontal loads is of extreme importance for the evaluation of seismic safety of masonry structures. In this paper, finite element analyses adopting different material models are presented, results are compared with experimental data and the accuracy of the analysed material models is investigated.

1 INTRODUCTION

Analysing composite materials, such as masonry, by means of homogeneous models (macromodels) remains a compulsory way for the calculation of the response of usual structures. The utilization of non homogeneous models (micromodels) for the representation of the real discontinuities of material, is conceptually more satisfactory but presents serious shortcomings because of the high number of dof required for the analysis of structures of usual dimensions and because of the necessity to know chemical-physical parameters whose evaluation is difficult and expensive.

In the case of masonry, the utilization of macromodels for the calculation of the response under vertical and seismic loads is particularly critical with respect to other materials, for example concrete, because of:

1) dimensions of inerts, which cannot be assumed "small" with respect to the dimensions of structural elements;

2) not casual geometry of the masonry type.

The use of macromodels for the study of masonry subject to vertical and seismic loads needs therefore a preventive calibration of mechanical parameters in order to reproduce, with a good approximation, the global experimental behaviour of structural elements subject to actions similar to the real ones.

In this paper, the behaviour of the following macromodels for the study of masonry panels subject to vertical and lateral loads is investigated: the no-tension model (NT), the constant tensile strength model (CTS) and the linear tensile strength model (LTS). Beyond these displacement-based models, the behaviour of a stress-based finite element is investigated; this element, presented in (Braga and Liberatore (1990, 1991)), is based on the no-tension hypothesis and on the discretization of the stress field by means of a finite number of fan stress fields (multiple fan element or MF). The comparison among these models and some experimental results of racking tests is dealt with in terms of axial force-shear domains, and it allows to draw useful informations about the practical applicability of the above mentioned models.

2 SAFETY DOMAINS

A parallelepiped panel of width b, height h and thickness t is considered (fig. 1). If it is assumed that the lower and upper faces of the panel remain plane in the deformed configuration, the displacement field can be represented by only 6 generalized displacement components, which are collected in the vector **u** (fig. 2):

$$u = (u_1 \quad v_1 \quad \phi_1 \quad u_2 \quad v_2 \quad \phi_2)^T \tag{1}$$

The corresponding vector of generalized forces **f** is (fig. 3):

$$f = (T_1 \quad N_1 \quad M_1 \quad T_2 \quad N_2 \quad M_2)^T \tag{2}$$

The minimum principal stresses at the vertices of the panel are collected in the matrix S (fig. 4):

$$S = \begin{bmatrix} \sigma_{11} & \sigma_{12} \\ \sigma_{21} & \sigma_{22} \end{bmatrix} \tag{3}$$

The displacement vector can be expressed by the superposition of 3 rigid displacements: u_0 (lateral), v_0 (vertical), and φ_0 (rotation) (fig. 5):

$$u_0 = \frac{u_1 + u_2}{2} \tag{4a}$$

$$v_0 = \frac{v_1 + v_2}{2} \tag{4b}$$

$$\phi_0 = \frac{\phi_1 + \phi_2}{2} \tag{4c}$$

and of 3 strain components: Δu (shear), Δv (axial) and $\Delta\varphi$ (bending) (fig. 6):

$$\Delta u = u_2 - u_1 + \phi_0 h \tag{5a}$$

$$\Delta v = v_2 - v_1 \qquad (5b)$$

$$\Delta\phi = \phi_2 - \phi_1 \qquad (5c)$$

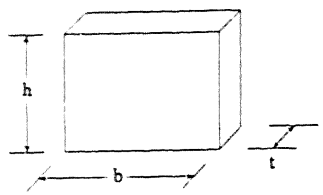

Figure 1. Masonry panel

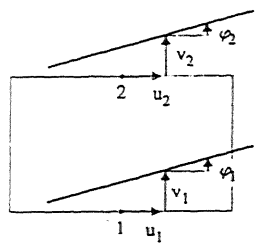

Figure 2. Displacements

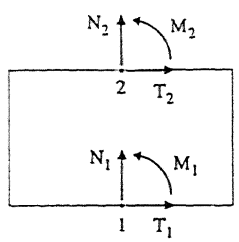

Figure 3. Forces

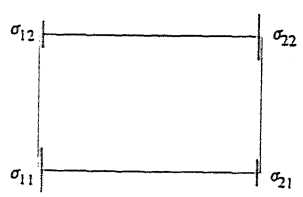

Figure 4. Minimum principal stresses at vertices

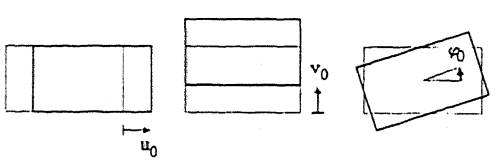

Figure 5. Rigid displacements

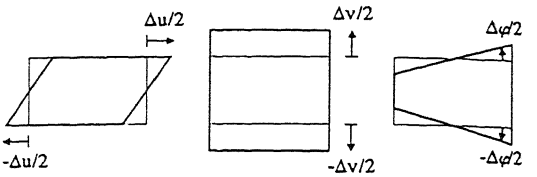

Figure 6. Strain components

Only strain components will be considered since rigid displacements do not produce any stress. It is also useful to introduce the dimensionless strain components ε_1, ε_2, ε_3:

$$\varepsilon_1 = \frac{\Delta u}{b} \qquad (6a)$$

$$\varepsilon_2 = \frac{\Delta v}{b} \qquad (6b)$$

$$\varepsilon_3 = \Delta\phi \qquad (6c)$$

The analysis can be conveniently carried out if a system of spherical co-ordinates ρ (radius), η (latitude) and ξ (longitude) is introduced in the space of dimensionless strains (fig. 7):

$$\varepsilon_1 = \rho\cos\eta\cos\xi \qquad (7a)$$

$$\varepsilon_2 = \rho\sin\eta \qquad (7b)$$

$$\varepsilon_3 = \rho\cos\eta\sin\xi \qquad (7c)$$

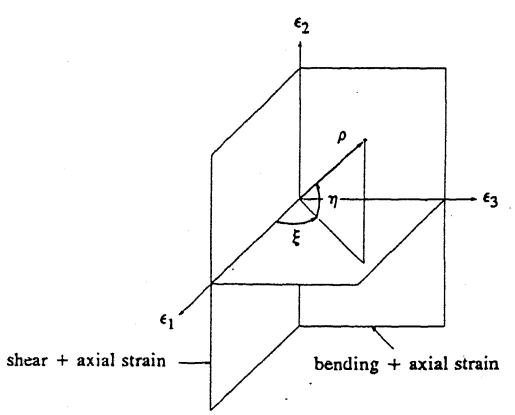

Figure 7. Systems of co-ordinates in strain space

In the space of dimensionless strains, the plane ξ=0 contains the fields of shear + axial strain, while the plane ξ=π/2 contains the fields of bending + axial strain.

Since in usual situations only tension-compression states of stress arise in the panel, on the basis of the experimental results presented in (Dhanasekar, Kleeman, Page (1985)), a linear elastic stress-strain law with Young's modulus E and tensile cut-off is assumed. The tensile strength is equal to zero for models MF and NT; it is equal to the uniaxial tensile strength for the CTS model, and it is linearly ranging between σ_t to $0.25\sigma_t$ for the LTS model when the minimum principal stress σ_1 ranges from 0 to the uniaxial compressive strength $-\sigma_k$ (fig. 8).

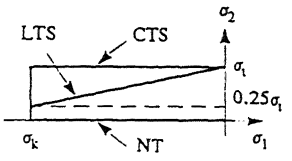

Figure 8. Tensile cut-off laws

Safety domains can be conveniently defined in terms of dimensionless axial force α and of dimensionless shear β:

$$\alpha = -\frac{N_2}{b t \sigma_k} \qquad (8a)$$

$$\beta = \frac{T_2}{b t \sigma_k} \qquad (8b)$$

If it is assumed that the panel crisis occurs because of the reaching of the compressive strength σ_k, and as the minimum principal stress occurs to one of the vertices, crisis condition can be written as follows:

$$\max_{ij}(-\sigma_{ij}) = \sigma_k \qquad (i,j = 1,2)\,(9)$$

Singling out of critical strain fields can be carried out for a generic couple (η, ξ) by increasing the value of ρ from zero until to reach the crisis condition. The critical value ρ_k is function of η and ξ; therefore the set of the terns (ρ_k, η, ξ) is the set of the strain fields corresponding to the frontier of safety domain; if for such strain fields we calculate the values of axial force N_{2k} and of shear force T_{2k}, and the corresponding dimensionless values α_k and β_k:

$$\alpha_k = -\frac{N_{2k}}{b t \sigma_k} \qquad (10a)$$

$$\beta_k = \frac{T_{2k}}{b t \sigma_k} \qquad (10b)$$

the set of the couples (α_k, β_k) represents the frontier of safety domain.

Calculation of safety domains can be conveniently carried out by introducing a reference panel with unit width, thickness and elastic modulus, height equal to μ=h/b, and subject to dimensionless strains (indicating all the quantities related to reference panel by a ') (fig. 9):

$$\rho' = 1, \quad \eta' = \eta, \quad \xi' = \xi \qquad (11)$$

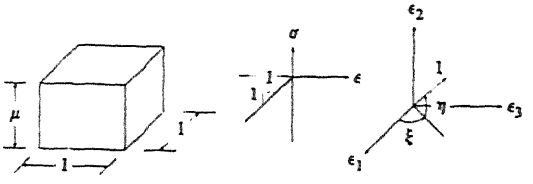

Figure 9. Reference panel

The similitude relationships between the actual panel and the reference panel are:

$$N_j = E b t \rho N_j' \qquad (j = 1,2)\,(12a)$$

$$T_j = E b t \rho T_j' \qquad (j = 1,2)\,(12b)$$

$$M_j = E b^2 t \rho M_j' \qquad (j = 1,2)\,(12c)$$

$$\sigma_{ij} = E \rho \sigma_{ij}' \qquad (i,j = 1,2)\,(12d)$$

The geometry of reference panel is defined only by the aspect ratio μ; and its strain field by η and ξ.

Crisis condition for reference panel has the following expression:

$$\max_{ij}(-\sigma_{ij}') = \frac{\sigma_k}{E \rho_k} = \sigma_k' \quad (i,j = 1,2)\,(13)$$

where the compressive strength of reference panel σ_k' is function of ρ_k. From the operational point of view, the research of ρ_k is carried out by decreasing the value of the compressive strength of reference panel, starting from very high values, until to reach the crisis condition; decreasing the compression strength results in shrinking of the material strength domain.

Dimensionless axial force α_k and shear β_k, can be written, using the similitude relationships:

$$\alpha_k = -\frac{N_{2k}'}{\sigma_k'} \qquad (14a)$$

$$\beta_k = \frac{T_{2k}'}{\sigma_k'} \qquad (14b)$$

From these expressions it can be noticed that the frontier of safety domain depends only on quantities related to reference panel. Applications which will be presented in the following paragraph are related to the situation of shear + axial strain (ξ=0), since in this case a wide experimental casuistry is available. In such situation the frontier of safety domain is a curve in the α-β plane, which depends on the aspect ratio and on the ratio between tensile and compressive strengths.

3 NUMERICAL APPLICATIONS AND COMPARISONS WITH EXPERIMENTAL DATA

The models utilized in numerical applications are divided in two categories:

a) displacement-based models (NT, CTS, LTS);

b) stress-based models (MF).

Displacement-based models satisfy everywhere kinematic equations, constitutive relationships are satisfied only in Gauss points, equilibrium equations are satisfied only in terms of nodal forces. Violation of constitutive relationships is particularly critic; in fact it leads to tensile stresses which are not compatible with the material strength domain and therefore to a systematic overvaluation of ultimate shear; in order to reduce this effect it is necessary to use very fine meshes with a high number of Gauss points in each element. The considerable degree of mesh refinement is also necessary in order to accurately take into account the discontinuities of stress field where tensile strength is exceeded, if this is different from 0, as for models CTS and LTS. Another critical point of displacement-based models is the calculation of the principal stress at the vertices of panel. As stress values, calculated by derivation of shape functions, are not very accurate (and this is much as true as more high the gradient of stress is, as at vertices), it is necessary to extrapolate the stress state at vertices from the stress states in the centre points of the nearest elements; in particular, the stress states of 6 elements have been utilized in numerical applications, resulting in a complete quadratic extrapolation of the 3 stress components σ_x, σ_y, τ_{xy}, from which minimum principal stress has been calculated. Response calculation has been carried out by equilibrium iterations based on the modified Newton-Raphson method.

MF stress-based element needs an extremely limited number of dof because only one element per panel is required, and it discretizes the stress field by a finite number of fan stress fields (fig. 10).

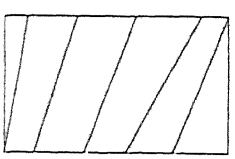

Figure 10. Multiple fan stress field

This element satisfies everywhere equilibrium equations and constitutive relationships but not, in general, kinematic equations. The position of elementary fans is determined, for a known displacement vector, by minimizing the total complementary energy. Values of axial force, of shear and of minimum principal stresses at vertices can be easily calculated when the positions of elementary fans are known.

The safety domains for μ=1 and μ=1.5 are shown in figs 11, 12 together with POR domain and with experimental results of racking test (Turnsek and Sheppard (1980)), having assumed σ_t=0.06σ_k (τ_k=0.04σ_k).

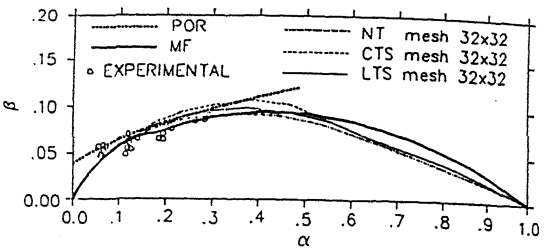

Figure 11. Safety domains (μ=1)

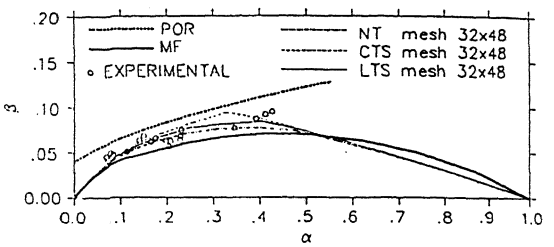

Figure 12. Safety domains (μ=1.5)

The number of elementary fans utilized for model MF is equal to 6; while elements with 4 nodes and with 9 Gauss points have been used for models NT, CTS and LTS in order to create a mesh 32x32 for μ=1 and 32x48 for μ=1.5.

In general, a good correlation can be observed among the different models, and between these and experimental results, with maximum differences comparable to the experimental dispersions. NT and CTS curves are a lower bound and an upper bound, respectively, of the LTS curve. The curves of model MF are nearly coincident with those of displacement-based models for low values of α, by going down below them in an intermedium range of α, and at last by going up them for high values of α. In practical situations (α=0.05-0.4), for μ=1 there is a very good correlation between the MF curve and experimental data, with a tendency to overvaluation from displacement-based models, while for μ=1.5 the curves of displacement-based models show a better correlation with experimental data, with a tendency to underestimate from MF curve. POR curve doesn't change as aspect ratio does, therefore it cannot take into account the systematic decreasing of ultimate shear when aspect ratio grows up.

The curves of model NT, for μ=1 and for different degrees of mesh refinement (16x16, 32x32, 50x50) are shown in fig. 13, together with the curves MF, POR and experimental data. It is possible to conclude that the mesh 32x32 is sufficiently accurate.

The stress states at the centre point of the elements of the mesh and at vertices for models CTS and LTS are shown in figs 14, 15 respectively; in abscisses and in ordinates there are the axes of the dimensionless principal stresses σ_1'/σ_k' and σ_2'/σ_k', respectively, of the reference panel. Those diagrams confirm the arising of tension-compression states, or of cracking-compression states if the tensile strength is exceeded; in the latter case the representative point lies on the axis $\sigma_2'/\sigma_k'=0$.

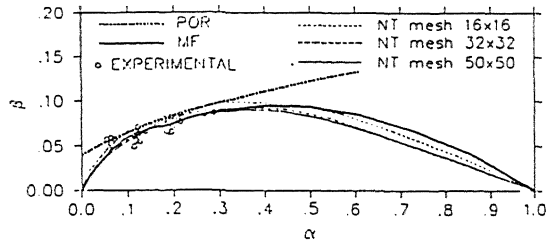

Figure 13. Influence of mesh on model NT

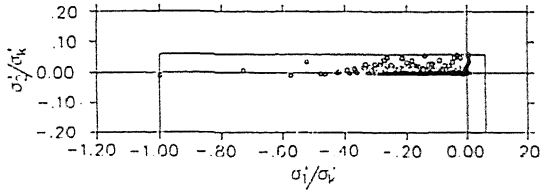

Figure 14. Stress states for model CTS

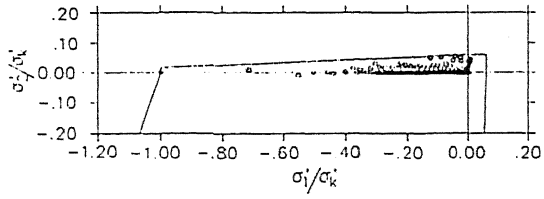

Figure 15. Stress states for model LTS

A representation of principal stresses in the centre point of each element of the mesh for models NT and CTS, $\mu=1$ and $\alpha=0.09$ is shown in fig. 16. In the representation of the model NT, the edges of the elementary fans of model MF are also shown. This representation confirms a substantial correlation among the different models.

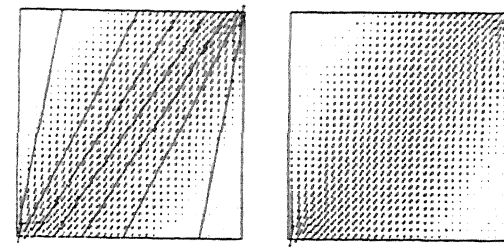

a) NT + MF b) CTS
Figure 16. Stress fields ($\mu=1$, $\alpha=0.09$)

4 CONCLUSIONS

The comparisons between numerical and experimental results showed that the greater number of dof and the greater complexity of the laws of the material strength domain of displacement-based models do not yield improvements of accuracy with respect to the stress-based model MF. Therefore, the substantial accuracy of model MF, together with its low computational cost, makes it particularly suitable for the analysis of complex masonry structures under vertical and seismic loads.

REFERENCES

Braga, F., Liberatore, D. 1990. A Finite Element for the Analysis of the Response of Masonry Buildings Under Seismic Actions. *Proc. of the 5th North American Masonry Conference*, Urbana.

Braga, F., Liberatore, D. 1990. Elastic Potential Energy, Forces and Stiffness of a No-Tension Panel. *Proc. of Istituto di Scienza e Tecnica delle Costruzioni*, n. 18 Potenza (in Italian).

Braga, F., Liberatore, D. 1991. Safety Domains of Masonry Panels Calculated According to the Multiple Fan Stress Field. *Proc. of the 5th Italian Conference on Earthquake Engineering*, Palermo (in Italian).

Braga, F., Liberatore, D. 1991. Modeling of Seismic Behaviour of Masonry Buildings. *Proc. of the 9th International Brick/Block Masonry Conference*, Berlin.

Dhanasekar, M., Kleeman, P.W., Page, A.W. 1985. Biaxial Stress-Strain Relations for Brick Masonry. *Journal of the Structural Div.*, ASCE, Vol. 111, No. ST5.

Turnsek, V., Sheppard, P. 1980. The Shear and Flexural Resistance of Masonry Walls. *International Research Conference on Earthquake Engineering*, Skopje.